



**QUEEN'S
UNIVERSITY
BELFAST**

Quantifying Aflatoxin B1 in peanut oil using fabricating fluorescence probes based on upconversion nanoparticles.

Sun, C., Li, H., Koidis, A., & Chen, Q. (2016). Quantifying Aflatoxin B1 in peanut oil using fabricating fluorescence probes based on upconversion nanoparticles. DOI: 10.1016/j.saa.2016.04.040

Published in:

SPECTROCHIMICA ACTA PART A-MOLECULAR AND BIOMOLECULAR SPECTROSCOPY

Document Version:

Peer reviewed version

Queen's University Belfast - Research Portal:

[Link to publication record in Queen's University Belfast Research Portal](#)

Publisher rights

Copyright 2016 Elsevier.

This manuscript is made available under a Creative Commons Attribution-NonCommercial-NoDerivs License (<https://creativecommons.org/licenses/by-nc-nd/4.0/>), which permits distribution and reproduction for non-commercial purposes, provided the author and source are cited.

General rights

Copyright for the publications made accessible via the Queen's University Belfast Research Portal is retained by the author(s) and / or other copyright owners and it is a condition of accessing these publications that users recognise and abide by the legal requirements associated with these rights.

Take down policy

The Research Portal is Queen's institutional repository that provides access to Queen's research output. Every effort has been made to ensure that content in the Research Portal does not infringe any person's rights, or applicable UK laws. If you discover content in the Research Portal that you believe breaches copyright or violates any law, please contact openaccess@qub.ac.uk.

1 Quantifying Aflatoxin B₁ in peanut oil using fabricating fluorescence probes
2 based on upconversion nanoparticles

3

4 **Cuicui Sun, Huanhuan Li, Anastasios Koidis, Quansheng Chen***

5 *School of Food and Biological engineering, Jiangsu University, Zhenjiang, 212013, P. R. China.*

6 *Institute for Global Food Security, Queen's University Belfast, BT95GN, Northern Ireland, United*
7 *Kingdom.*

8

* Corresponding author. Tel.: +86-511-88790318; fax: +86-511-88780201

E-mail: qschen@ujs.edu.cn (Qs Chen)

9 **ABSTRACT**

10 Rare earth doped upconversion nanoparticles convert near-infrared excitation light into visible
11 emission light. Compared to organic fluorophores and semiconducting nanoparticles, upconversion
12 nanoparticles (UCNPs) offer high photochemical stability, sharp emission bandwidths, and large
13 anti-Stokes shifts. Along with the significant light penetration depth and the absence of
14 autofluorescence in biological samples under infrared excitation, these UCNPs have attracted more
15 and more attention on toxin detection and biological labelling. Herein, the fluorescence probe based
16 on UCNPs was developed for quantifying Aflatoxin B₁ (AFB₁) in peanut oil. Based on a specific
17 immunity format, the detection limit for AFB₁ under optimal conditions was obtained as low as 0.2
18 ng·mL⁻¹, and in the effective detection range 0.2 to 100 ng·mL⁻¹, good relationship between
19 fluorescence intensity and AFB₁ concentration was achieved under the linear ratios up to 0.90.
20 Moreover, to check the feasibility of these probes on AFB₁ measurements in peanut oil, recovery
21 tests have been carried out. A good accuracy rating (%) was obtained in this study. results showed
22 that the nanoparticles can be successfully applied for sensing AFB₁ in daily edible oils.

23 **Keywords:** rapid toxin detection; biological labelling; upconversion nanoparticles; Fluorescence
24 probes

25

26 **1. Introduction**

27 China and India regions is the world's biggest market for peanut and its derivatives (in particular
28 peanut oil) in terms of productions well as consumption (Sanders Iii et al., 2014). Several survey
29 studies have shown that mold will grow quickly, and the possible presence of aflatoxins would
30 transfer into peanut oil, when peanuts are stored for weeks in humid conditions (Klu & Chen, 2015).
31 Aflatoxins are a group of highly toxic secondary metabolites produced mainly by *Aspergillus flavus*
32 and *Aspergillus parasiticus* on a variety of food products (K. Chen et al., 2014). These toxins are
33 known to be potent carcinogens, teratogens, mutagens, and immunosuppression and pose harmful
34 threat to animal and human health (Xia et al., 2013). Naturally occurring aflatoxins are composed of
35 B₁, B₂, G₁ and G₂ types. Among them, aflatoxin B₁ (AFB₁) is the most abundant and carcinogenic
36 (Passone, Girardi, & Etcheverry, 2013). Since peanut oil is widely consumed as diet in the Asian
37 region, even low levels of contamination may cause severe health and safety incidents (Luongo et al.,
38 2013; Quiles, Manyes, Luciano, Mañes, & Meca, 2015; Van de Perre, Jacxsens, Lachat, El Tahan, &
39 De Meulenaer, 2015). Therefore, determination of AFB₁ in peanut and its derivatives becomes a
40 subject of great importance for industries and regulators alike.

41 A wide range of methods are currently available, including thin layer chromatography (TLC),
42 spectrometry (Busman, Liu, Zhong, Bobell, & Maragos, 2014), gas chromatography(Ceker, Agar,
43 Alpsoy, Nardemir, & Kizil, 2014), High-performance liquid chromatography (HPLC)(Herzallah,
44 2009), fluorescence polarization assays(Maragos, 2009), radio immunoassays(Waliyar, Reddy, &
45 Lava-Kumar, 2009), enzyme-linked immunosorbent assay(Sai et al., 2010) (ELISA) and fiberoptic
46 based immunoassays(Kozlov et al., 2004), which have been used for the detection of aflatoxins.
47 However, most of these techniques require well equipped laboratories, trained personnel, harmful

48 solvents, and are time-consuming. Therefore, the demand for developing a rapid and sensitive
49 method for sensing aflatoxins is urgent.

50 In optical detection methods, conventional downconversion fluorescent materials, such as
51 semiconductor nanoparticles, dye-coupled hybrid materials and mesoporous silica, are fluorophores
52 that are commonly used in biological studies and clinical application because of their unique features
53 (Mnoyan, Kirakosyan, Kim, Jang, & Jeon, 2015); Sharma, Rawat, Solanki, & Bohidar, 2015). One
54 important intrinsic limitation, however, is that these materials usually emit one lower-energy photon
55 after absorption of a higher-energy ultraviolet or visible photon. This lead to significant
56 disadvantages, such as low light-penetration depth, potentially severe photodamage to living
57 organisms (Sozer & Kokini, 2014), and the autofluorescence (noise) of some biological samples. To
58 solve these problems, the development of alternative biological luminescent labels through the use of
59 up-converting rare-earth nanophosphors (UCNPs) has attracted a tremendous amount of attention
60 due to the unique luminescence properties of rare-earth nanoparticles. Lanthanide-doped,
61 near-infrared (NIR)-to-visible upconversion nanophosphors are capable of emitting strong visible
62 fluorescence under the excitation of NIR light (typically 980 nm). They have been shown to have
63 significant advantages as fluorescent bio-label (Boyer, Manseau, Murray, & van Veggel, 2010;
64 Chatterjee, Rufaihah, & Zhang, 2008; Fang et al., 2014; Huang, Yu, & Chu, 2015; Ma, Liu, Han,
65 Yang, & Liu, 2015; Tian et al., 2015) over the traditional organic fluorophores due to their attractive
66 optical and chemical features, including low toxicity (Chatterjee, Gnanasammandhan, & Zhang,
67 2010; Zhang, Wu, Tang, Su, & Lv, 2014), large stokes shifts (Ahn et al., 2016), high resistance to
68 photobleaching (Feng Wang et al., 2011), blinking, photochemical stability (H. Q. Chen, Yuan, &
69 Wang, 2013) and the lack of both auto-fluorescence (Aramburu et al., 2015) and light scattering

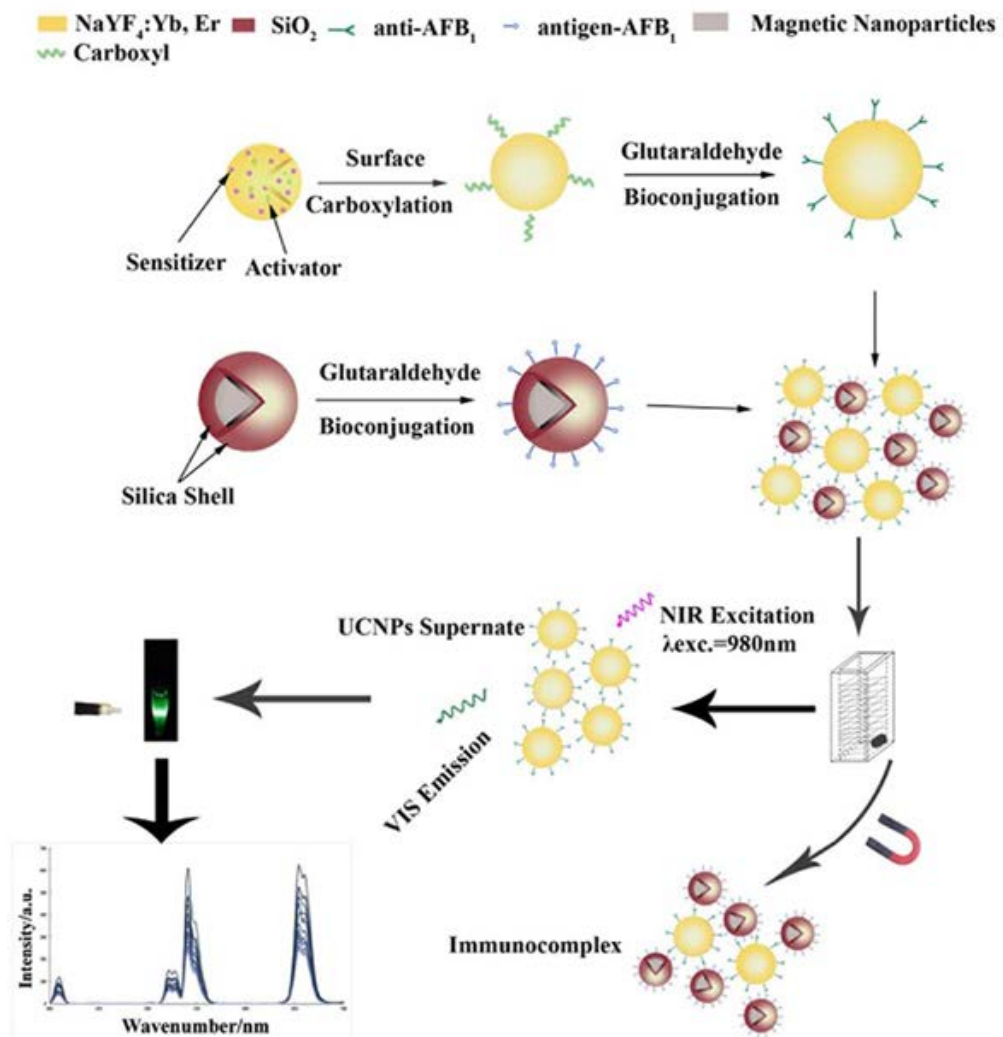
70 background (Zhou, Liu, & Li, 2012). As a result, the signal-to-background ratio and sensitivity of the
71 detection can be greatly improved. Moreover, upconversion nanoparticles have also attracted
72 increasing interest due to their optical properties which can be achieved by adding a $\lambda_{exc.} = 980$ nm
73 optical source used in fluorescence measurement. From the mentioned advantages above, we can
74 conclude that the upconversion nanophosphors as color label has a high potential on the detection of
75 toxin.

76 In recent years, with the rapid development of nanostructured materials and nanotechnology in
77 the fields of biotechnology and contaminat detection, magnetic nanoparticles (MNPs) have been
78 receiving considerable attention. Due to their magnetic properties, low toxicity, and biocompatibility,
79 MNPs are useful for the separation of target antibiotics from a mixture of antibiotics and matrix
80 substances. Additionally, MNPs help to concentrate the separated antibiotics into a small volume,
81 which is suitable for impedance measurements(Z. Wang et al., 2013). Artificial antigen-modified
82 MNPs were employed as immune sensing probes, and antibody functionalized UCNPs were used as
83 signal probes; the antibodies-functionalized UCNPs were linked to the surface of the MNPs by
84 antibody–antigen affinity.

85 Herein, we explored a novel and sensitive fluorescence probe for sensing toxin by crosslinking
86 rare earth doped upconversion nanoparticles and immunoproteins. Fig. 1 presents the scheme of this
87 proposed fluorescence bioassay platform. Specific procedures are outlined as follows. (1)
88 Upconversion nanoparticles (UCNPs) were synthesized and functionalized. (2) The resultant
89 water-soluble UCNPs were conjugated with anti-AFB₁ antibodies to produce biological fluorescent
90 probes. (3) A fluorescence standard curve was prepared with different concentrations of AFB₁. (4)
91 Independent food samples were tested. As an efficient, specific, and technically simple biological

92 probe, these selective sensors can be used for rapidly detecting toxin in food.

93



94

95

96

Fig. 1. Scheme of this proposed fluorescence bioassay platform.

97

98 2. Materials and methods

99 2.1 Instruments

100 The size and morphology of nanoparticles were determined using a JEM-2100HR transmission
101 electron microscope (TEM, JEOL Ltd., Japan). X-ray diffraction (XRD) measurements were
102 performed using a D8-advance instrument (Bruker AXS Ltd., Germany). Upconversion fluorescence

103 spectra were measured using an F-7200 fluorescence spectrophotometer (Hitachi Co., U.S.A.)
104 modified with an external 980nm laser (Beijing Hi-Tech Optoelectronic Co., China) instead of the
105 internal excitation source. Fourier transform infrared spectrophotometer (FT-IR) spectra of the
106 nanoparticles were obtained with a Nicolet Nexus 470 (Thermo Electron Co., U.S.A.) using a KBr
107 detector.

108 *2.2 Reagents*

109 AFB₁ standard solution, (8 mg·mL⁻¹ solution in methanol and working dilution by deionized
110 water), AFB₁-BSA antigen (extent of labeling 8-12 mol Aflatoxin B₁ per mol BSA), monoclonal
111 anti-AFB₁ antibody, (6 mg·mL⁻¹ solution and working dilution by phosphate buffer solution) was
112 obtained from Beijing Mozhidong Bio-tech (city. Country). Hydrated rare earth nitrate (RECl₃·xH₂O,
113 RE Y, Yb, Er, ≥ 99.99%), oleic acid (≥ 90%) and octadecanoic acid (≥ 90%) were purchased from
114 Sigma-Aldrich (Shanghai, China). In addition, FeCl₃·6H₂O, sodium fluoride, sodium hydroxide,
115 methyl alcohol, toluene, ethyl alcohol, sodium citrate, 1,6-hexanediamine, anhydrous sodium acetate,
116 glycol, bovine serum albumin (BSA, 96-99%), 25% glutaraldehyde, tetraethyl orthosilicate (TEOS ≥
117 98%), and 3-aminopropyltrimethoxysilane (APTES) was all purchased from Sinopharm Chemical
118 Reagent Co., Ltd. (Shanghai, China). All the chemicals used were of analytical grade. The water used
119 was deionized.

120 *2.3 Synthesis and surface modification of rare-earth-doped*

121 Oleic acid-capped NaYF₄: Yb, Er UCNPs were synthesized according to the method reported in
122 predecessors' research (F. Wang et al., 2010) with a few modifications. In a typical experiment, 2 ml
123 of RECl₃ (0.2 M, RE = Y (78%), Yb (20%), Er (2%)) in methanol were added to a 50 ml flask
124 containing 3 ml oleic acid and 7 ml 1-octadecene, and the solution was heated to 160 °C for 30 min

125 and then cooled down to room temperature. Thereafter, 5 ml methanol solution of NH_4F (1.6 mmol)
126 and NaOH (1 mmol) was added and the solution was stirred for 30 min. After methanol evaporated,
127 the solution was heated to $300\text{ }^\circ\text{C}$ under argon for 1.5 h and cooled down to room temperature. The
128 resulting nanoparticles were precipitated by the addition of ethanol, collected by centrifugation,
129 washed with methanol and ethanol several times, and finally dried in an oven at $60\text{ }^\circ\text{C}$.

130 The obtained oleic acid-capped UCNPs can disperse well in nonpolar solvents. However, for
131 biological applications, hydrophobic UCNPs should be converted into hydrophilic UCNPs so as to
132 be compatible with biomolecules, such as antibodies. Thus, surface modification of the hydrophobic
133 UCNPs was performed via a ligand exchange process as described in predecessors' research (Ong,
134 Ang, Alonso, & Zhang, 2014). Briefly, a mixture of 2 mmol sodium citrate in 15 ml of diethylene
135 glycol was first heated to $110\text{ }^\circ\text{C}$ under argon for 30 min. Oleic acid-capped UCNPs (10 mg)
136 dispersed in cyclohexane and toluene were then added into the mixture and the reaction was heated
137 to $160\text{ }^\circ\text{C}$ for evaporation of cyclohexane and toluene. After complete evaporation, the reaction was
138 further maintained at $160\text{ }^\circ\text{C}$ for 3 h. Water-soluble UCNPs were then collected by centrifugation,
139 washed with ethanol and ultrapure water several times, and finally dispersed in ultrapure water.

140

141 *2.4 Preparation of amine-functionalized Fe_3O_4 magnetic nanoparticles*

142 Amine-functionalized Fe_3O_4 MNPs were prepared according to Gao's work (Gao, Gu, & Xu,
143 2009). Briefly, a solution of 6.5 g 1,6-hexanediamine, 2.0 g anhydrous sodium acetate and 1.0 g
144 $\text{FeCl}_3 \cdot 6\text{H}_2\text{O}$ as a ferric source in 30 mL glycol was stirred vigorously at $50\text{ }^\circ\text{C}$ to give a transparent
145 solution. This solution was then transferred into a Teflon-lined autoclave and reacted at $198\text{ }^\circ\text{C}$ for 6
146 h. The MNPs were then rinsed with water and ethanol (2 or 3 times) to effectively remove the

147 solvent and unbound 1,6-hexanediamine, and then dried at 50 °C before characterization and
148 application. During each rinsing step, the nanoparticles were separated from the supernatant by using
149 magnetic force.

150 *2.5 Preparation of immunosensing probes and signal probes*

151 The artificial antigen conjugated MNPs and antibody conjugated immunosensing probes were
152 fabricated with the classical glutaraldehyde method. Typically, 10 mg of MNPs were dispersed in 5
153 mL of 10 mmol/L phosphate buffer solution (pH 7.4) by ultrasonication for 20 min. 1.25 mL of 25%
154 glutaraldehyde was then added to the mixture. The mixture was shaken slowly at room temperature
155 for 1 h, and the Fe₃O₄ MNPs were separated by an external magnetic field and washed with PBS
156 three times to remove the physically adsorbed glutaraldehyde. Subsequently, 11.67 μL of AFB₁-BSA
157 antigen, at a concentration of 6 mg mL⁻¹, was added into 5 mL of a suspension of Fe₃O₄ MNPs in
158 PBS. The mixture was shaken slowly for 6 h at room temperature. The surplus biomolecules were
159 removed by magnetic separation of the particles from the solution. The AFB₁-BSA antigen
160 conjugated MNPs were treated with 5 mL BSA at 3% concentration in 10 mmol/L PBS at room
161 temperature for 6 h to block the unreacted and nonspecific sites. Finally, the as-prepared probes were
162 stored in 5 mL of 10 mmol/L PBS at 4 °C prior to use. The biofunctionalization of amino-modified,
163 water-soluble UCNPs conjugated with monoclonal antibody, namely the preparation of the signal
164 probes, was similar to that of the antigen conjugated MNPs described above. The prepared antigen
165 conjugated Fe₃O₄ MNPs and antibody functionalized UCNPs were characterized by FT-IR
166 spectroscopy.

167 *2.6 Sample preparation and measurement*

168 Twelve naturally contaminated peanut oil samples obtained from local supermarkets were

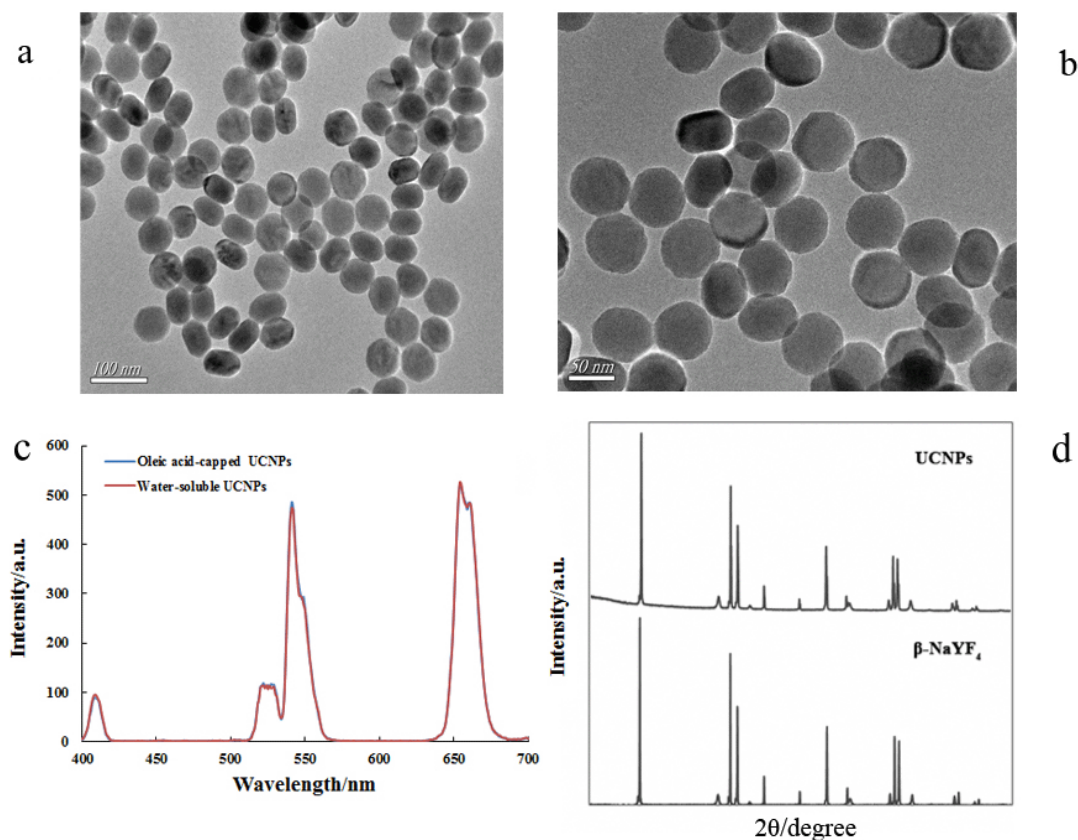
169 treated according to official methods of China (*GB/T, 2003*) with some modifications. Briefly, five
170 grams of each peanut oil sample and 5 g NaCl were introduced into a 100 mL flask, and the
171 extracting solution (methanol:water; 7:3 (v:v)) was filled to the mark, completely mixed with the
172 compound and then the mixture was transferred into the cup of a homogenizer. The mixture was then
173 stirred at high-speed and extracted for 2 min. Next, the resulting solution was filtered, and 10 mL of
174 filtrate was transferred into a 50 mL flask; water was filled to the mark, and the flask contents were
175 mixed to homogeneity. The resulting mixture was further filtered with glass fiber filter paper until
176 the filtrate was clear. For the standard addition and recovery experiments, the AFB₁ standard
177 solutions were added to the peanut oil samples before adding the extracting solution. After the
178 complete chemical reaction and magnetism separation, fluorescence spectra of the obtained
179 supernatants (from 400 to 700 nm) were measured with a fluorescence spectrophotometer equipped
180 with a 980 nm laser excitation under the excitation power (1.3 W). Here, the 541nm peak intensity
181 emission wavelength was used.

182 **3. Results and Discussion**

183 *3.1 Characterization of the prepared upconversion nanoparticles and magnetic nanoparticles*

184 Results showed that toxin-specific antibodies with high selectivity and sensitivity were
185 successfully conjugated onto the surface of UCNPs to yield UCNP–antibody probes, as illustrated in
186 Fig.1. Prior to the conjugation, the precursor UCNPs were first characterized by transmission
187 electron microscopy (TEM), X-ray diffraction (XRD) and fluorescence spectral measurements, as
188 shown in Fig 2. Successful surface modification, selectivities, sizes, and luminance and spectral
189 properties of UCNPs before and after surface modification were validated by TEM and fluorescence
190 spectral measurements, as presented in Fig.2 (a, b, c). The TEM images confirmed the hexagonal

191 UCNP structures and revealed that the particles were uniform with an average diameter of
192 approximately 50 nm before and after surface modification and bioconjugation. The fluorescence
193 spectra of the UCNPs showed the expected characteristic emission peaks at approximately 407, 542,
194 and 657 nm upon NIR (980 nm) excitation, corresponding to blue, green, and red light, respectively
195 (the naked-eye images in the inset show the visible intensity of the UCNPs). The peaks are ascribed
196 to the transitions from the $^2H_{9/2}$, $^4S_{3/2}$, and $^4F_{9/2}$ levels to the $^4I_{15/2}$ ground state of the Er^{3+} ion (L.
197 Wang, Li, & Li, 2007; Leyu Wang & Li, 2006). The fluorescence properties were also retained, as
198 both the oleic acid-capped UCNPs and the water-soluble UCNPs showed the same characteristic
199 emission peaks upon NIR excitation. Additionally, the diffraction peaks of the XRD pattern in Fig. 2
200 (d) were identified as pure hexagonal β -phase $NaYF_4$ crystals (JCPDS Standard Card No. 16-0334);
201 no diffraction peaks corresponding to cubic phase crystals or other impurities were observed.



202

203 **Fig. 2.** TEM images of oleic acid-capped UCNPs (a) and water-soluble UCNPs (b), Fluorescence properties of

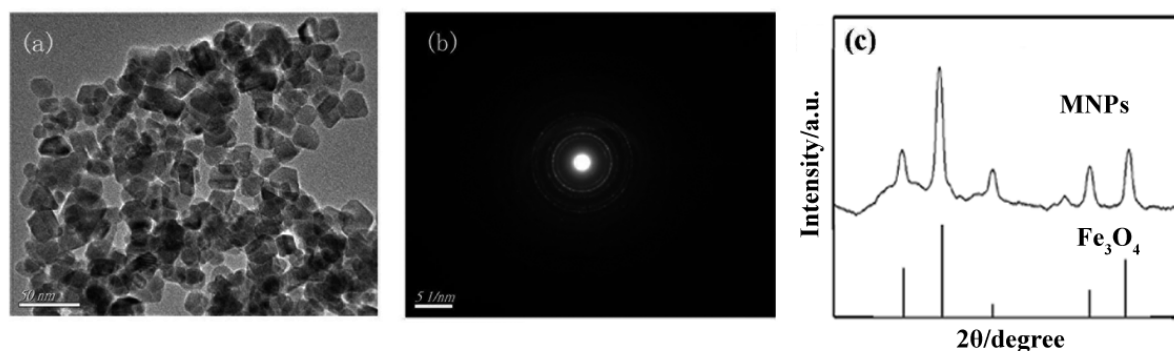
204 oleic acid-capped UCNPs and water-soluble UCNPs (c), XRD pattern of oleic acid-capped UCNPs (d).

205

206 The UCNPs used in this work were Yb, Er ion-pair doped hexagonal phase NaYF₄
207 nanoparticles. The hexagonal phase NaYF₄ was reported to be one of the most efficient hosts for
208 performing infrared to visible photon conversion when activated by Yb, Er ion-pairs. During the
209 experiment, we found that the reaction time and temperature were the two main influential factors in
210 the phase transition of NaYF₄ UCNPs. In order to obtain hexagonal phase NaYF₄, the reaction was
211 maintained at 300 °C for 1.5 h.

212 The XRD pattern of NaYF₄: Yb, Er phosphor gives several reflections shown in Fig.2 (d) indicates
213 that the microballoon sphere are well-crystallized. In Yb³⁺ and Er³⁺ co-doped systems, Yb³⁺ ions act
214 as sensitizers and Er³⁺ ions as activators. The Debye Scherrer formula was used to calculate the
215 crystallite size of the synthesized phosphor and is given by $d = \frac{0.89\lambda}{\beta \cos \theta}$, where d is the crystallite size,
216 λ is the wavelength of the X-rays, β is full width at half maximum and θ is the diffraction angle. The
217 average value of the crystallite size was found to be around 50 nm that confirms the formation of
218 nanostructured crystallites.

219 Fig. 3 (a, b) displays the TEM and selected area electron diffraction (SAED) images of
220 amino-modified MNPs confirming good dispersibility and morphology with an average size of about
221 20 nm. In addition, the crystalline structure and phase purity was determined by powder XRD as
222 shown in Fig. 3 (c). The positions and relative intensities of all diffraction peaks matched well with
223 those from the JCPDS card (No.52-0102) for magnetite. The sharp, strong peaks confirmed the
224 products were well crystallized.



225

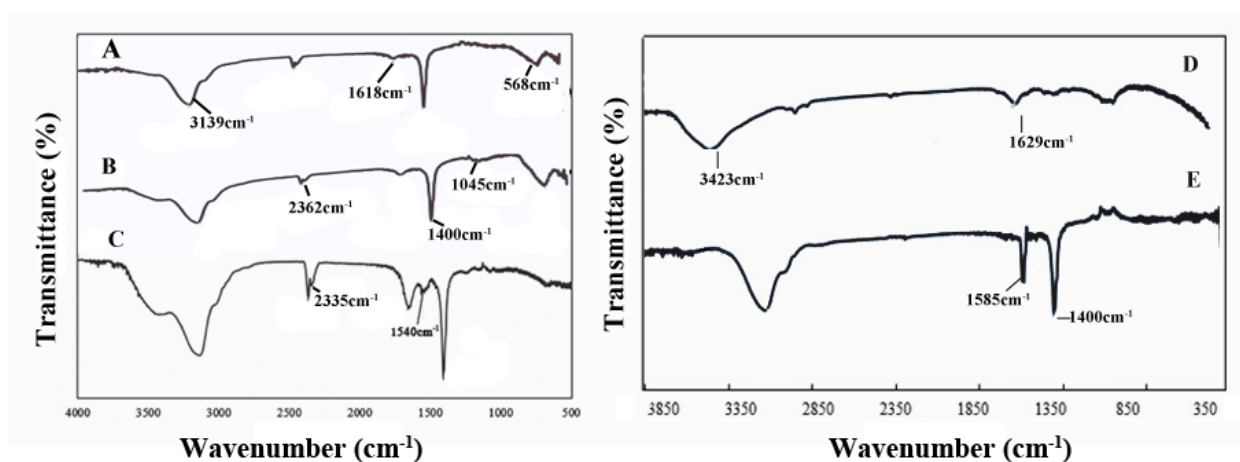
226 **Fig. 3.** TEM image (a), SAED image (b), and XRD (c) of the amino-functionalized magnetic nanoparticles.

227

228 *3.2 Characterization of the antigen modified MNPs and antibody functionalized UCNPs*

229 In this report, to verify the formation of the bionanoparticles, infrared spectroscopy was utilized
 230 to monitor the reaction products in each derivatization step, and the results are shown in Fig. 4:
 231 spectra of UCNPs (A), carboxylation-UCNPs (B), carboxylation-UCNPs–antibody probes (C),
 232 amination-MNPs (D) and amination-MNPs-antigen. Fig. 4 (A, B, C, D and E) confirmed the
 233 presence of carboxyl on the UCNPs, UCNP-antibody probes, UCNP-antibody-antigen-MNPs
 234 compounds and antigen on the MNPs. More specifically, in Fig. 4 (A, B, C), the water-soluble
 235 UCNPs presented with a single broad peak at 3427 cm^{-1} , corresponding to the stretching vibration of
 236 hydroxide radicals (-OH). The characteristic peak at 1629 cm^{-1} is related to the asymmetric
 237 stretching vibration of carboxyl groups (-COOH) of the citrate ligands on the surface of the UCNPs.
 238 These two peaks indicated that the carboxyl groups from the ligand exchange were successfully
 239 modified on the surface of UCNPs to produce water-soluble UCNPs. When the glutaraldehyde
 240 crosslinking method -prepared antibodies were introduced, three characteristic peaks at 2360, 2335,
 241 and 1396 cm^{-1} appeared. The peaks at 2360 and 2335 cm^{-1} corresponded to methylene stretching
 242 vibrations (-CH₂-). The peak at 1396 cm^{-1} corresponded to carboxyl stretching vibrations (COO-)

243 due to the linking reaction between the water-soluble UCNPs and the antibodies. Furthermore, a new
244 peak was observed at 1540 cm^{-1} upon comparison of the spectra of the
245 UCNP-antibody-antigen-MNPs complex and the UCNP-antibody probe; this peak is attributed to
246 the distinct amide I and amide II vibration modes characteristic of antigen proteins. On the other
247 hand, in Fig. 4 (D, E), a new peak was observed at 1400 cm^{-1} upon comparison of the spectra of the
248 amino-MNPs complex and the MNPs-antigen probes; this peak is attributed to the distinct amide I
249 and amide II vibration modes characteristic of antigen proteins. In the FT-IR spectra of
250 antigen-functionalized- Fe_3O_4 MNPs and antibody-functionalized-UCNPs, all the characterized peaks
251 of Fe_3O_4 MNPs and UCNPs appeared in the corresponding wavenumbers, indicating the
252 modification of antigen and antibody onto the surface of MNPs and UCNPs. On the basis of these
253 characterizations, the proposed UCNP-based method is suitable for sensing toxin.



254

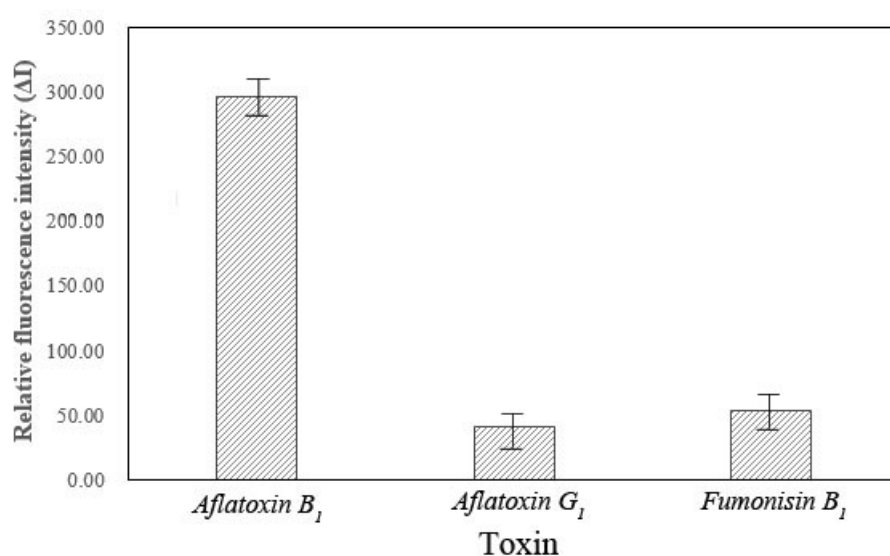
255 **Fig.4.** FT-IR spectrums of oleic acid-capped UCNPs (A), carboxylation-UCNPs (B),
256 carboxylation-UCNPs-antibody probes (C), amination-MNPs (D) and amination-MNPs-antigen (E).

257 3.3 Specific Capturing Evaluation

258 In order to evaluate the specificity of the immunoassay procedure using this developed
259 fluorescent probe for AFB_1 , other two commonly occurring toxins, Aflatoxin G_1 (AFG_1) and

260 Fumonisin B₁ (FB₁) were examined, instead of AFB₁, with the developed fluorescent probe. Results
261 were shown in Fig. 5, both AFG₁ and FB₁ caused negligible changes of the fluorescence, while a
262 significant change of fluorescence was observed for AFB₁. Therefore, it is clearly demonstrated that
263 the designed fluorescent probe has good specificity to capture AFB₁.

264



265

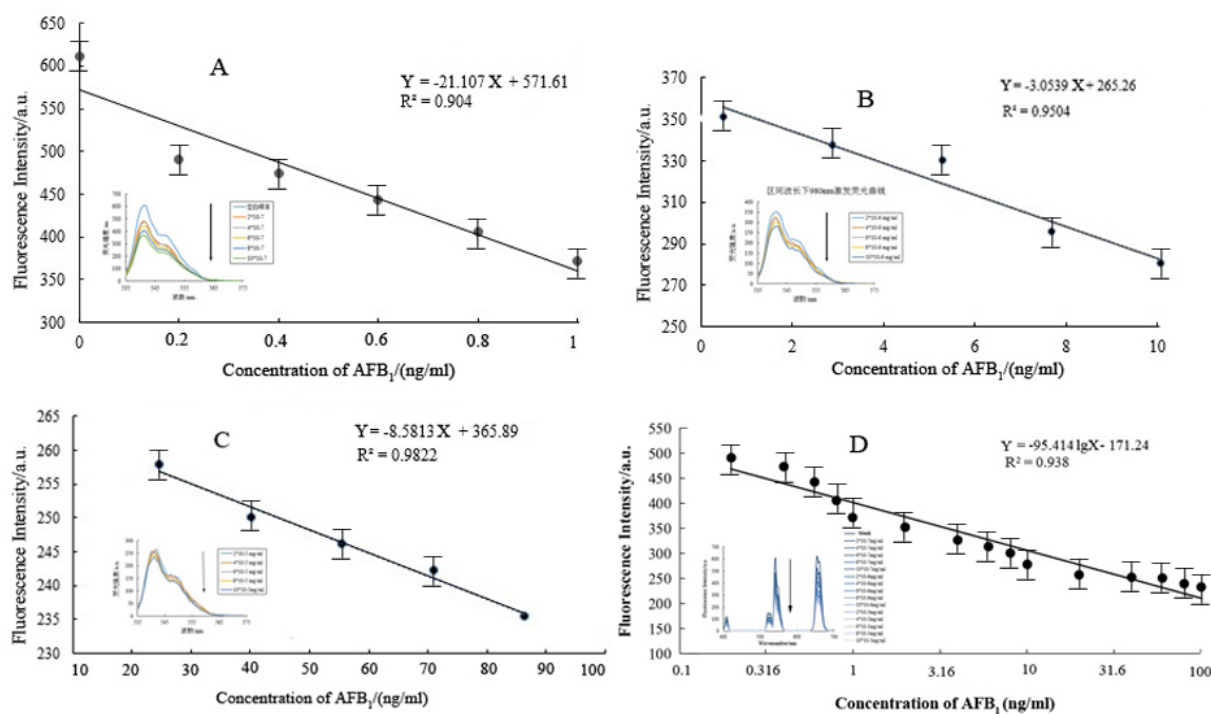
266 **Fig. 5.** Specific selectivity evaluation of the proposed method for AFB₁ (1 ng·ml⁻¹) against other toxin (1 ng·ml⁻¹).

267

268 3.4 Analytical performance

269 In a typical experiment, different concentrations of AFB₁ were incubated under agitation with
270 the UCNP-antibody probes for 2 h at 37 °C. On the basis of the specificity of the antibody for the
271 AFB₁, UCNPs-antibody-antigen-MNPs complexes were formed. The samples were subsequently
272 concentrated and separated by magnetic for 10 min to separate the unbound UCNPs-antibody probes.
273 Thereafter, serial dilutions of the supernatants were prepared to examine the fluorescence spectra of
274 the complexes. The 541 nm emission peak excited by a 980 nm laser was used to monitor the AFB₁
275 concentration (Lu, Chen, Wang, Zheng, & Li, 2015).

276 As shown in Fig. 6 (A, B, C, D), the fluorescence intensity rapidly decreased as the AFB₁
277 concentration increased from 0.2 to 100 ng·mL⁻¹. A strong linear correlation ($R^2 = 0.938$) was
278 obtained between various concentrations of AFB₁ (X) and the upconversion luminescent intensity
279 (Fig. 6D). In thinner, secondary, and high three separate concentration phases, linear ratios are all
280 higher than 0.90. It can be seen (Fig. 6) that fluorescence intensity has a minimum linear relationship
281 with lowest concentrations ($R^2 = 0.904$), which is due to the UCNPs nano-particles detection
282 precision; fluorescence intensity has a best linear relationship with high concentrations of AFB₁ (R^2
283 $= 0.9822$) because of the dense solution and immunization specific recognition precision. The
284 detection limit of this proposed method for AFB₁ was found to be 0.2 ng·mL⁻¹. The precision
285 expressed as the relative standard deviation (RSD) of this detection is 3.56% (obtained from a series
286 of 10 standard samples each containing 0.4 ng·mL⁻¹). Fig. 6 also depicts a typical recording output
287 for the detection of AFB₁ with different concentrations. Overall, these results demonstrate that the
288 developed method applied here have a good potential to be used as a rapid screening for the
289 detection of mycotoxin ingrain crops.



290

291 **Fig. 6.** Linear relation between upconversion luminescent intensity and the various concentrations of AFB₁.

292

293 Statistical analysis revealed that the detection limit of AFB₁ are equal to 0.2 ng·mL⁻¹, as
 294 estimated by using 3σ. These values are desirable for detection AFB₁ in various kinds of foods
 295 relative to the maximum acceptable standards of these mycotoxins in China and other countries. The
 296 RSD of AFB₁ detection was equal to 3.56% indicating that the developed method exhibited good
 297 reproducibility. In the absence of AFB₁-BSA-MNPs, the fluorescence intensity of NaYF₄: Yb, Er
 298 was at a maximum, and in the presence of AFB₁-BSA-MNPs, the antigen binds with
 299 antibody-AFB₁-UCNPs and causes the fluorescent signal of the unreleased UCNPs gradually
 300 decreased. It can be understood as that the more MNPs-antigen- antibody-UCNPs was formed, the
 301 fewer antibody-UCNPs were remained, and the fluorescence intensity is weaker.

302 To check feasibility of this method, the accuracy of the measurements of AFB₁ in peanut oil was
 303 also evaluated by determining the recovery of AFB₁.by adding a known quantity of standard solution

304 to the test solution. As shown in Table 1, the recoveries of AFB₁ were between 90.1% and 113.4%,
305 indicating a high level of accuracy of the developed immunoassay. These analyses demonstrated that
306 the proposed method could be applied to the analysis of AFB₁ in real agricultural commodities.

307

308 **Table 1:** Recovery results for AFB₁ detection

Samples	Background concentration (ng·ml ⁻¹)	Added concentration (ng·ml ⁻¹)	Detected concentration (ng·ml ⁻¹) (mean±SD)	Recovery ratio%
AFB ₁	0.052	0.1	0.150±0.032	98
AFB ₁	0.052	1	0.98±0.120	92.8
AFB ₁	0.734	0.5	1.301±0.233	113.4
AFB ₁	0.734	1	1.720±0.121	98.6
AFB ₁	3.364	1	4.265±0.236	90.1
AFB ₁	3.364	5	8.465±0.103	102.02

309

310 **4. Conclusions**

311 In this study, rare earth doped upconversion nanoparticles have been successfully assembled for
312 sensing Aflatoxins B₁ in actual food samples (peanut oil). Herein, antigen-modified magnetic
313 nanoparticles were used for immunosensing probes, and antibody functionalized NaYF₄
314 upconversion nanoparticles as color signal probes. Due to strong fluorescence signal, low
315 autofluorescence of the UCNPs, rapid separation and purification of the magnetic nanoparticles and
316 the immunocomplex, this method can reduce significantly the overall assay time. Based on these
317 results, the ease of use and reliability, the developed method could be extended for the rapid
318 detection of other toxins in the edible oils and other agricultural products. suggest that it maybe be
319 extended to other agriculture products

320

321

322 **Acknowledgments**

323 This work has been financially supported by the National Natural Science Foundation of China
324 (31471646) and a Project Funded by the Priority Academic Program Development of Jiangsu Higher
325 Education Institutions (PAPD).

326

327 **Conflict of interest**

328 The authors declare no conflicts of interest. The authors alone are responsible for the content of
329 this manuscript.

330

331 **References**

- 332 Ahn, K.S., Lim, K. R., Jeong, D., Lee, B. Y., Kim, K. S., & Lee, W.Y. (2016). Fluorescence energy transfer inhibition
333 bioassay for cholera toxin based on galactose-stabilized gold nanoparticles and amine-terminated quantum dots.
334 *Microchemical Journal*, 124, 9-14.
- 335 Aramburu, I., Galban, J., Ostra, M., Ubide, C., Vidal, M., & Zuriarrain, J. (2015). Uncertainty in CCD detectors with and
336 without cooling devices when used for molecular fluorescence measurements. *Analytical Methods*, 7(6),
337 2379-2385.
- 338 Boyer, J.C., Manseau, M.P., Murray, J. I., & van Veggel, F. C. J. M. (2010). Surface Modification of Upconverting
339 NaYF₄ Nanoparticles with PEG-Phosphate Ligands for NIR (800 nm) Biolabeling within the Biological
340 Window. *Langmuir*, 26(2), 1157-1164.
- 341 Busman, M., Liu, J., Zhong, H., Bobell, J. R., & Maragos, C. M. (2014). Determination of the aflatoxin AFB1 from corn
342 by direct analysis in real time-mass spectrometry (DART-MS). *Food Additives & Contaminants: Part A*, 31(5),
343 932-939.
- 344 Ceker, S., Agar, G., Alpsoy, L., Nardemir, G., & Kizil, H. E. (2014). Antagonistic effects of *Satureja hortensis* essential
345 oil against AFB₁ on human lymphocytes in vitro. *Cytology and Genetics*, 48(5), 327-332.
- 346 Chatterjee, D. K., Gnanasammandhan, M. K., & Zhang, Y. (2010). Small Upconverting Fluorescent Nanoparticles for
347 Biomedical Applications. *Small*, 6(24), 2781-2795.
- 348 Chatterjee, D. K., Rufaihah, A. J., & Zhang, Y. (2008). Upconversion fluorescence imaging of cells and small animals
349 using lanthanide doped nanocrystals. *Biomaterials*, 29(7), 937-943.
- 350 Chen, H.Q., Yuan, F., & Wang, L. (2013). Simple and sensitive turn-on luminescent detection of biothiols based on
351 energy transfer between green-emitting upconversion nanocrystals and gold nanoparticles. *Analytical Methods*,
352 5(11), 2873-2879.
- 353 Chen, K., Fang, J., Peng, X., Cui, H., Chen, J., Wang, F., Zhou, Y. (2014). Effect of selenium supplementation on
354 aflatoxin B₁-induced histopathological lesions and apoptosis in bursa of Fabricius in broilers. *Food and*
355 *Chemical Toxicology*, 74, 91-97.
- 356 Fang, S., Wang, C., Xiang, J., Cheng, L., Song, X., Xu, L., Liu, Z. (2014). Aptamer-conjugated upconversion nanoprobe
357 assisted by magnetic separation for effective isolation and sensitive detection of circulating tumor cells. *Nano*
358 *Research*, 7(9), 1327-1336.
- 359 Gao, J., Gu, H., & Xu, B. (2009). Multifunctional Magnetic Nanoparticles: Design, Synthesis, and Biomedical
360 Applications. *Accounts of Chemical Research*, 42(8), 1097-1107.
- 361 Herzallah, S. M. (2009). Determination of aflatoxins in eggs, milk, meat and meat products using HPLC fluorescent and
362 UV detectors. *Food Chemistry*, 114(3), 1141-1146.
- 363 Huang, L.J., Yu, R.Q., & Chu, X. (2015). DNA-functionalized upconversion nanoparticles as biosensors for rapid,
364 sensitive, and selective detection of Hg²⁺ in complex matrices. *Analyst*, 140(15), 4987-4990.
- 365 Karimi, M., Habibi-Rezaei, M., Safari, M., Moosavi-Movahedi, A. A., Sayyah, M., Sadeghi, R., & Kokini, J. (2014).
366 Immobilization of endo-inulinase on poly-d-lysine coated CaCO₃ micro-particles. *Food Research International*,
367 66, 485-492.
- 368 Klu, Y. A. K., & Chen, J. (2015). Effect of peanut butter matrices on the fate of probiotics during simulated
369 gastrointestinal passage. *LWT - Food Science and Technology*, 62(2), 983-988.
- 370 Kozlov, I. A., Melnyk, P. C., Stromsborg, K. E., Chee, M. S., Barker, D. L., & Zhao, C. (2004). Efficient strategies for the
371 conjugation of oligonucleotides to antibodies enabling highly sensitive protein detection. *Biopolymers*, 73(5),
372 621-630.
- 373 Lu, Z., Chen, X., Wang, Y., Zheng, X., & Li, C. (2015). Aptamer based fluorescence recovery assay for aflatoxin B₁

374 using a quencher system composed of quantum dots and graphene oxide. *Microchimica Acta*, 182(3-4),
375 571-578.

376 Luongo, D., Russo, R., Balestrieri, A., Marzocco, S., Bergamo, P., & Severino, L. (2013). In vitro study of AFB₁ and
377 AFM₁ effects on human lymphoblastoid Jurkat T-cell model. *Journal of immunotoxicology*, 11(4), 353-358.

378 Ma, Y., Liu, H., Han, Z., Yang, L., & Liu, J. (2015). Highly-reproducible Raman scattering of NaYF₄:Yb,Er@SiO₂@Ag
379 for methylamphetamine detection under near-infrared laser excitation. *Analyst*, 140(15), 5268-5275.

380 Maragos, C. (2009). Fluorescence polarization immunoassay of mycotoxins: a review. *Toxins*, 1(2), 196-207.

381 Mnoyan, A. N., Kirakosyan, A. G., Kim, H., Jang, H. S., & Jeon, D. Y. (2015). Electrostatic Stabilized InP Colloidal
382 Quantum Dots with High Photoluminescence Efficiency. *Langmuir*, 31(25), 7117-7121.

383 Ong, L. C., Ang, L. Y., Alonso, S., & Zhang, Y. (2014). Bacterial imaging with photostable upconversion fluorescent
384 nanoparticles. *Biomaterials*, 35(9), 2987-2998.

385 Passone, M. A., Girardi, N. S., & Etcheverry, M. (2013). Antifungal and antiaflatoxic activity by vapor contact of
386 three essential oils, and effects of environmental factors on their efficacy. *LWT - Food Science and Technology*,
387 53(2), 434-444.

388 Quiles, J. M., Manyes, L., Luciano, F., Mañes, J., & Meca, G. (2015). Influence of the antimicrobial compound allyl
389 isothiocyanate against the *Aspergillus parasiticus* growth and its aflatoxins production in pizza crust. *Food and
390 Chemical Toxicology*, 83, 222-228.

391 Sai, N., Chen, Y., Liu, N., Yu, G., Su, P., Feng, Y., Gao, Z. (2010). A sensitive immunoassay based on direct hapten
392 coated format and biotin-streptavidin system for the detection of chloramphenicol. *Talanta*, 82(4), 1113-1121.

393 Sanders Iii, C. T., DeMasie, C. L., Kerr, W. L., Hargrove, J. L., Pegg, R. B., & Swanson, R. B. (2014). Peanut
394 skins-fortified peanut butters: Effects on consumer acceptability and quality characteristics. *LWT - Food Science
395 and Technology*, 59(1), 222-228.

396 Sharma, A., Rawat, K., Solanki, P. R., & Bohidar, H. B. (2015). Electrochemical response of agar ionogels towards
397 glucose detection. *Analytical Methods*, 7(14), 5876-5885.

398 Sozer, N., & Kokini, J. L. (2014). Use of quantum nanodot crystals as imaging probes for cereal proteins. *Food Research
399 International*, 57, 142-151.

400 Tian, J., Bai, J., Peng, Y., Qie, Z., Zhao, Y., Ning, B., Gao, Z. (2015). A core-shell-structured molecularly imprinted
401 polymer on upconverting nanoparticles for selective and sensitive fluorescence sensing of sulfamethazine.
402 *Analyst*, 140(15), 5301-5307.

403 Van de Perre, E., Jacxsens, L., Lachat, C., El Tahan, F., & De Meulenaer, B. (2015). Impact of maximum levels in
404 European legislation on exposure of mycotoxins in dried products: Case of aflatoxin B1 and ochratoxin A in
405 nuts and dried fruits. *Food and Chemical Toxicology*, 75, 112-117.

406 Waliyar, F., Reddy, S., & Lava-Kumar, P. (2009). Review of immunological methods for the quantification of aflatoxins
407 in peanut and other foods. *Journal Information*, 36(1), 54-59.

408 Wang, F., Deng, R., Wang, J., Wang, Q., Han, Y., Zhu, H., Liu, X. (2011). Tuning upconversion through energy migration
409 in core-shell nanoparticles. *Nat Mater*, 10(12), 968-973.

410 Wang, F., Han, Y., Lim, C. S., Lu, Y. H., Wang, J., Xu, J., Liu, X. G. (2010). Simultaneous phase and size control of
411 upconversion nanocrystals through lanthanide doping. *Nature*, 463(7284), 1061-1065.

412 Wang, L., Li, P., & Li, Y. (2007). Down- and Up-Conversion Luminescent Nanorods. *Advanced Materials*, 19(20),
413 3304-3307.

414 Wang, L., & Li, Y. (2006). Na(Y_{1.5}Na_{0.5})F₆ Single-Crystal Nanorods as Multicolor Luminescent Materials. *Nano Letters*,
415 6(8), 1645-1649.

416 Wang, Z., Yue, T., Yuan, Y., Cai, R., Niu, C., & Guo, C. (2013). Preparation of immunomagnetic nanoparticles for the
417 separation and enrichment of *Alicyclobacillus* spp. in apple juice. *Food Research International*, 54(1), 302-310.

418 Xia, Q., Huang, X.Y., Xue, F., Zhang, J.J., Zhai, B., Kong, D.C., Long, X.D. (2013). Genetic polymorphisms of DNA
419 repair genes and DNA repair capacity related to aflatoxin b₁ (AFB₁)-induced DNA damages. *New Research*
420 *Directions in DNA Repair*, 1, 377-412.

421 Xu, X., Liu, X., Li, Y., & Ying, Y. (2013). A simple and rapid optical biosensor for detection of aflatoxin B₁ based on
422 competitive dispersion of gold nanorods. *Biosensors and Bioelectronics*, 47(0), 361-367.

423 Yang, B.c., Wang, F., Deng, W., Zou, Y., Liu, F.y., Wan, X.d., Huang, O.p. (2015). Wooden-tip electrospray ionization
424 mass spectrometry for trace analysis of toxic and hazardous compounds in food samples. *Analytical Methods*,
425 7(14), 5886-5890.

426 Zhang, Y., Wu, L., Tang, Y., Su, Y., & Lv, Y. (2014). An upconversion fluorescence based turn-on probe for detecting
427 lead(ii) ions.. *Analytical Methods*, 6(22), 9073-9077.

428 Zhou, J., Liu, Z., & Li, F. (2012). Upconversion nanophosphors for small-animal imaging. *Chemical Society Reviews*,
429 41(3), 1323-1349.

430

431